From Natural Attapulgite to Mesoporous Materials: Methodology, Characterization and Structural Evolution

Huaming Yang,*,†,‡ Aidong Tang,§ Jing Ouyang,† Mei Li,‡ and Stephen Mann*,‡

Department of Inorganic Materials, School of Resources Processing and Bioengineering, Central South University, Changsha 410083, P. R. China, Centre for Organized Matter Chemistry, School of Chemistry, University of Bristol, Bristol BS8 1TS, U.K., and School of Chemistry and Chemical Engineering, Central South University, Changsha 410083, P. R. China

Received: December 4, 2009; Revised Manuscript Received: January 11, 2010

In this paper, we report the synthesis of hexagonally ordered aluminum-containing mesoporous silica, Al-MCM-41, from natural attapulgite (Al-substituted $Si_8O_{20}Mg_5(OH)_2(H_2O)_4 \cdot 4H_2O$) without addition of silica or aluminum reagents. A pretreatment process involving sequential mechanical grinding and acid leaching is critical to the successful use of attapulgite as a source of both Si and Al in the surfactant-templated hydrothermal synthesis of Al-MCM-41. The resulting mesophase had a surface area of 1030 m^2/g and an average pore diameter of 3.7 nm with narrow pore size distribution. The influence of changes in processing parameters, such as grinding time, hydrothermal conditions, and calcination temperature, on the textural characteristics of the Al-MCM-41 products is studied. Investigations of the mechanism of structural evolution indicate that grinding of attapulgite results in amorphization and partial structural breakdown, transformation of the fibrous mineral bundles into rod-shaped particles, and partial displacement of octahedrally coordinated Al^{3+} ions into the Si−O tetrahedral framework. Subsequent acid etching dissolves the Mg-rich octahedral sheets to produce samples with variable texture due to modifications in the residual aluminum-containing silicate sheets and associated silica fragments. Solid-state magic-angle spinning NMR spectroscopy indicates that Al^{3+} ions are located in both octahedral and tetrahedral sites in the as-synthesized Al-MCM-41 samples, but that the calcined products consist primarily of Al^{3+} ions substituted in the tetrahedrally coordinated silica matrix of the ordered channel wall structure.

Introduction

The unprecedented discovery of a family of mesoporous silicas designated as M41S was reported by scientists at Mobil Research & Development Corporation in 1992.[1] One of the members of this extensive family, MCM-41, shows a hexagonal arrangement of uniform mesopores whose pore dimensions can be engineered from about 1.5 nm to larger than 10 nm in diameter, depending on the template and synthesis parameters.[2] These materials have attracted considerable interest in materials science and other relevant fields due to their large internal surface, high thermal and hydrothermal stability, possibility of controlling the pore dimension, and their potential acidity. For example, MCM-41 is a promising material for applications in catalysis, sensing, separation science, host−guest chemistry, environmental control, and drug delivery.[3−10]

The usual method for MCM-41 preparation is to employ a tetraalkoxysilane, such as tetramethylorthosilicate (TMOS) or tetraethylorthosilicate (TEOS), as the silica source. The use of these organic reagents has potential environmental consequences, particularly if high throughput, high-efficient synthesis processes are to be developed for the large scale production of various mesoporous silicas. Recently, attempts have been made to develop a green synthesis of MCM-41 by replacing potentially toxic organosilicates with inorganic colloidal silica, commercial amorphous silica, fumed silica, flashed dried precipitated silica, or natural silicate minerals.[11−19] In particular, the possibility of preparing MCM-41 from natural layered silicates has been emphasized due to abundant resources and similarity of the structural units to those of mesoporous materials. Yanagisawa et al. first reported the successful preparation of mesoporous silica from a layered silicate;[20] the results showed that reaction of the single layered polysilicate kanemite ($NaHSi_2O_5 \cdot 3H_2O$) with alkyltrimethylammonium chloride solutions resulted in the formation of alkyltrimethylammonium−kanemite complexes, which after calcination produced microporous products with pore diameters of 2−4 nm and surface areas of ca. 900 m^2/g. Subsequently, Fukushima and Inagaki developed this method and synthesized ordered mesoporous materials from natural kanemite,[21,22] Kang et al. used water glass and metakaolin as silica and aluminum sources to prepare Al-MCM-41 with a surface area of 877 m^2/g,[23] and Wang et al. reported the synthesis of mesoporous materials MCM-41 (surface area = 753 m^2/g) using metakaolin and TEOS as aluminum and silica sources, respectively.[15] In addition, high thermally stable Al-MCM-41 (surface area = 800 m^2/g) was obtained in situ in the presence of alkaline Na-montmorillonite and high amounts of surfactant.[24] Recent results by Tang et al. indicated that highly stable mesoporous materials (surface area = 576 m^2/g, average pore diameter = 4.83 nm) could be obtained via microwave-radiating a mixture of sodium silicate, aluminum chloride, and bentonite.[25]

Layered silicates are useful for the preparation of mesoporous materials as they serve both as a matrix and source of Si and

* Corresponding author. Tel: +86-731-8883 0549; fax: +86-731-8871 0804; e-mail: hmyang9392@hotmail.com (H.Y.), s.mann@bristol.ac.uk (S.M.).

† School of Resources Processing and Bioengineering, Central South University.

‡ University of Bristol.

§ School of Chemistry and Chemical Engineering, Central South University.

10.1021/jp911516b
Published on Web 02/01/2010

Al precursors. The mineral, attapulgite ($Si_8O_{20}Mg_5(OH)_2(H_2O)_4 \cdot 4H_2O$), is a hydrated magnesium silicate with fibrous morphology, whose structure was first reported by Bradley.[26] It consists of a double chain of Si−O tetrahedra running parallel to the long axis. Upper and lower parts of each double chain are linked by a layer of octahedral magnesium atoms in 6-fold coordination. The chains form a network of strips that are joined together only along the edges. Overall, the structure resembles a channeled wall where every second brick is missing.[27] Significantly, the natural mineral has a variable composition because of partial replacement of magnesium by aluminum, iron, and other elements. The presence of trivalent cations in the octahedral sites produces an excess of positive charge that is compensated by vacancies, thereby conferring dioctahedral characteristics to the mineral. The high surface area and porosity, thermal resistance, and fibrous morphology of attapulgite provide much potential for diverse applications such as catalyst supports, nanocomposites, and environmental absorbents.[28−33] Recently, Shi et al. reported the preparation of mesoporous-rich carbons by using attapulgite as templates and furfuryl alcohol as the carbon source through a vapor deposition polymerization method,[34] but there are few reports to the best of our knowledge concerning the use of this mineral for the preparation of mesoporous materials.

In this paper, we demonstrate a synthetic route to aluminum-containing hexagonally ordered mesoporous silicas (Al-MCM-41) from natural attapulgite without addition of silica or aluminum reagents. We investigate the use of physicochemical pretreatments (grinding and acid etching), followed by hydrothermal synthesis in the presence of the cationic surfactant, cetyltrimethylammonium bromide (CTAB), to prepare a range of mesoporous materials. In each case, the preparation parameters are discussed, and the samples characterized in detail by X-ray diffraction (XRD), thermogravimetric differential scanning calorimetry (TG-DSC), N_2 adsorption−desorption, transmission electron microscopy (TEM), high-resolution TEM (HRTEM), field-emission scanning electron microscopy (FESEM), Fourier transform infrared spectroscopy (FTIR), and ^{29}Si and ^{27}Al magic-angle spinning (MAS) solid state NMR spectroscopies. In addition, several aspects of the structural evolution from attapulgite to mesoporous silica are investigated, and a general synthesis mechanism is proposed.

Experimental Section

Synthesis. Attapulgite was obtained from Xuyi, China, and had the following chemical composition (wt %): SiO_2, 53.64; MgO, 11.87; Al_2O_3, 7.45; Fe_2O_3, 2.68; CaO, 2.11; K_2O, 0.46; Na_2O, 0.082; TiO_2 0.53; MnO, 0.078; H_2O, 10.05 (see Table 2). Grinding pretreatment was performed in a KM-10 planetary mill (Nanjing University Instrument Plant, China) at 800 rpm for 2 h with batches of 40 g attapulgite and 10 mm diameter stainless balls at a ball-to-sample weight ratio of 10:1. The milling chamber used had a net volume of about 1 L. The ground sample (1 g) was then treated with 100 mL of 8 M HCl (Sigma-Adrich) at 80 °C for 2 h, and cooled to room temperature. The suspension was filtered and thoroughly washed with deionized water to remove Cl^-, and dried at 80 °C for 12 h in air to form the acid-leached sample (white powder). The acid-leached sample was then used as direct silica and aluminum sources to prepare mesoporous silica (MCM-41). For this, 0.2 g of CTAB (99.0%, Aldrich) was dissolved in 10 mL of deionized water, and the acid-leached powder (0.2 g) was added to form a mixture. Sodium hydroxide (NaOH) solution (0.5 M, Fluka) was added dropwise to adjust the pH value of the mixture to 12.0. The mixture was stirred at 60 °C for 2 h in an oil bath and then transferred into a Teflon-lined steel autoclave, statically heated at 100 °C for 24 h, and cooled to room temperature. The resultant product was filtered, thoroughly washed with deionized water and anhydrous ethanol, and dried at 80 °C for 12 h to produce the as-synthesized sample. Subsequent calcination of the as-synthesized sample at 540 °C for 6 h in air with a heating rate of 2 °C/min in a furnace produced a white powder of Al-MCM-41.

Characterization. Wide angle X-ray diffraction (WAXRD) measurements were carried out using a Bruker Advance powder diffractometer with Cu Kα radiation ($\lambda = 0.15406$ nm). Small angle X-ray diffraction (SAXRD) patterns were recorded on Rigaku D/max 2550 using Cu Kα radiation ($\lambda = 0.15406$ nm) over the scanning range $2\theta = 1-10°$ at a voltage of 40 kV and 200 mA with a step width of 0.01°. TG-DSC was performed in air using a Netzsch STA 409EP simultaneous thermal analyzer at a heating rate of 5 °C/min. HRTEM was carried out on a FEI TECNAI G^2 20 electron microscope operating at an accelerating voltage of 200 kV. TEM (JEOL JEM-1200EX, 120 kV) was used for morphological analysis of the samples. FESEM images were collected using a JEOL JSM-6330F electron microscope. Nitrogen gas adsorption−desorption isotherms were measured at 77K using an ASAP 2020 unit. Prior to the sorption experiment, the samples were vacuum-dried at 200 °C for 10 h. The specific surface area was estimated by the multipoint Brunauer−Emmett−Teller (BET) method using the adsorption data, and the pore size distribution was determined by the Barrett−Joyner−Halenda (BJH) method using the desorption isotherm. The total pore volume was obtained from the maximum amount of nitrogen gas adsorbed at partial pressure ($P/P_0 = 0.999$). FTIR spectra of the samples were obtained on a PERKIN ELMER Spectrum One FTIR spectrometer using KBr discs in the range of 4000−400 cm^{-1}. Solid-state MAS NMR spectra were acquired at 7.1 T using Varian InfinityPlus 300 spectrometer with rotors 7.5 mm in diameter spun at 4.0 kHz for ^{29}Si, and 4 mm spun at 8.0 kHz for ^{27}Al. ^{29}Si MAS NMR spectra were recorded at a frequency of 59.6 MHz with 15 s recycle delay, while ^{27}Al spectra were obtained at 78.1 MHz with 2.0 s recycle delay.

Results and Discussion

Characterization of MCM-41 Products. Hydrothermal reaction of pretreated attapulgite with alkaline aqueous CTAB solutions resulted in a white powder with a Si/Al molar ratio of 12.6 according to the chemical analysis. SAXRD patterns of the calcined samples showed an intense (100) diffraction peak at $2\theta = 2.12°$ together with an additional (110) peak ($2\theta = 4.02°$) and a weak (200) peak at 4.6° (Figure 1), which were consistent with an aluminum-containing hexagonally ordered MCM-41 mesoporous structure.[1] HRTEM images of the calcined sample confirmed the presence of a hexagonally ordered mesopore arrangement with pore size of 3.5−3.8 nm (Figure 1, inset).

The hexagonal (*P6mm* space group) unit cell parameters (a_0; calculated according to the equation $a_0 = 2d_{100}/\sqrt{3}$), BET surface area measurements (typically 1030 m^2/g), and other structural aspects for samples calcined at different reaction temperatures and times are listed in Table 1. When the hydrothermal time was increased to 48 h at 100 °C, the (100) reflection shifted to a lower 2θ value (Figure 2a,b), indicating an increase in the unit cell parameter and a decrease in pore wall thickness.[13] On the other hand, the characteristic (110) reflection was absent after hydrothermal treatment at 160 °C

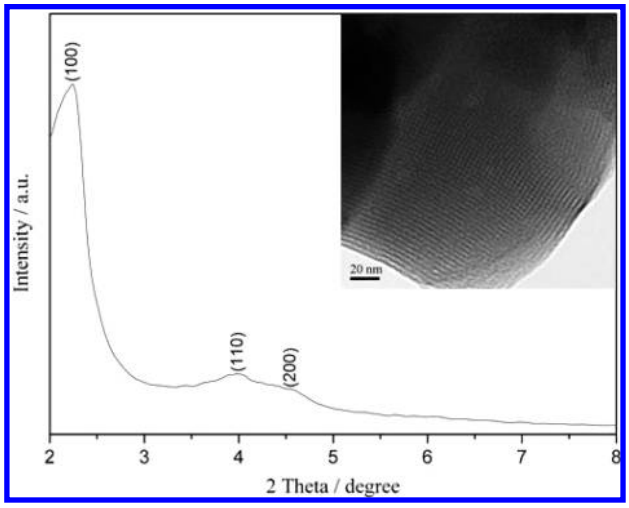

Figure 1. SAXRD pattern and HRTEM image (insert) of calcined Al-MCM-41.

for 24 h (Figure 2c), suggesting that formation of the hexagonal micellar arrays was inhibited at higher temperature.

TG-DSC analysis was performed to investigate the thermal behavior of the as-synthesized samples during calcination. The DSC profile was typical of MCM-41 (Figure 3), and showed two endothermal peaks at 305 °C and 346 °C, resulting from decomposition of the surfactant and subsequent hydrocarbon chain degradation; a narrow peak at 485 °C was mainly due to the combustion of the residual carbon. TG measurements indicated that the as-synthesized silica−surfactant material comprised approximately 56 wt % of silica.

The above results clearly indicated that natural attapulgite could be readily used to prepare Al-MCM-41 mesoporous materials. In general, the results indicated that the calcined products produced from attapulgite were similar to materials synthesized by conventional routes using chemical reactants.[2,35] For example, the pore volume of the mesoporous samples ranged from 0.95 to 1.15 mL/g compared with a range of 0.7−1.2 mL/g for mesostructured silicas prepared using tetraalkoxysilanes.[2] On the other hand, the pore wall thickness (1.10 nm) of the attapulgite-derived Al-MCM-41 was larger than the value (∼0.60 nm) usually obtained for MCM-41 materials prepared from pristine silica.[36,37]

Structural Aspects of Attapulgite Pretreatment: WAXRD Analysis. Four stages were required to successfully produce mesoporous silica from natural attapulgite. Using conditions described in the Experimental Section, hydrothermal treatment of the acid-leached attapulgite prepared without grinding failed to obtain the expected mesoporous materials (Table S1 and Figure S1, Supporting Information). Instead, the acid-leached and as-synthesized samples still retained the same structure as the original attapulgite (Figure S2), and, as a consequence, some minor peaks associated with natural attapulgite remained in the WAXRD profile of the calcined sample. Thus, grinding played a critical role in the transfer of natural attapulgite to Al-MCM-41.

The effect of grinding was investigated by WAXRD studies (Figure 4). The results indicated that reflections for attapulgite became absent within 2 h of grinding to produce an amorphous material. Formation of the disordered solid facilitated subsequent leaching of the octahedrally coordinated Mg sheets.[38,39] Defining a crystallinity index as $C = B_0I/(I_0B) \times 100\%$, where C is degree of crystallinity, and B_0 and B, or I_0 and I are background or peak intensities for nonground attapulgite and attapulgite, respectively,[40] indicated that only the maximum basal diffraction (110) peak showed appreciable crystallinity ($C = 31.5\%$) after 2 h grinding. In contrast, the (200), (130), (231), and (161) diffraction peaks were too weak to be measured, indicating that preferential distortion of the basal peaks was evidenced by the broadening of the (110) spacing during mechanical treatment, and that prolonged grinding enhanced amorphization of the attapulgite structure.

In general, particle size diminution, defects, and microstrains in the crystal structure produced during grinding can cause an increase in the background and broadening of the XRD peaks, with their final disappearance after long grinding times indicating a gradual breaking-down of the structure.[41] This phenomenon has also been reported for the grinding of other clay minerals including pyrophyllite, sepiolite, and talc.[41−43] From the above analysis, it is evident that attapulgite is very susceptible to structural alteration by grinding. Dry ball grinding produces impact, attrition, shear and compression forces, which together induce structural transformation of the material.[44] In particular, impact forces play a role in the rupture of particles, and attrition acts between the wall of the planetary mill, ball, and sample; on the other hand, the formation of structural alteration is readily affected by shear and compression.

The presence of Al^{3+} in the octahedral sheets of clays such as montmorillonite, orthochlorite, kaolin, and vermiculite affects the reactivity of these minerals to acid leaching,[45] although this appeared to have no effect on the ground samples of attapulgite (Figure 4). Chemical analyses indicated that the amount of SiO_2 in the acid-leached sample increased by 38.5% compared to unground attapulgite due to substantial loss of Mg and Fe (95.2% and 87.3%, respectively). In contrast, acid-induced loss of Al was lower (32.6%) with approximately 5 wt % (as Al_2O_3) remaining in the etched material. The results were consistent with the known M−O (M = Mg, Fe, Al) bond strengths[46] and the order of activation energies for acid extraction of these cations.[45] According to Gonzalez et al.,[47] acid attack progressively dissolves the octahedral sheet, creating micropores between the tetrahedral silicate sheets, and the resulting extraction of cations (Mg^{2+}, Fe^{3+} and Al^{3+}) from octahedral positions also promotes partial dissolution of the silicate framework to produce amorphous SiO_2 colloids. This was confirmed by WAXRD studies of samples produced after hydrothermally processing the acid-leached attapulgite with CTAB under basic conditions, which showed that both the as-synthesized and calcined materials were amorphous on the molecular scale (Figure 4).

Porosity Measurements. Figure 5 shows the N_2 adsorption−desorption isotherms of samples during the preparation of Al-MCM-41 from natural attapulgite. On the basis of the IUPAC classification, the isotherm of the calcined sample exhibited a typical type IV class with a H1-type hysteresis loop characteristic of MCM-41 mesoporous materials with one-dimensional cylindrical channels. The significant adsorption at lower P/P_0 was due to monolayer coverage of the mesoporous walls and not to the presence of microporous phases.[2] The appearance of a hysteresis loop below a relative pressure of 0.3 may be partially attributed to the instability of a liquid nitrogen meniscus for N_2 adsorption investigations performed at 77 K, whereas the gradual increase in the volume with P/P_0 was due to multilayer adsorption on the outer surface of the particles. A sharp inflection at $P/P_0 = 0.3-0.4$ was clearly observed in the calcined Al-MCM-41 isotherm, and corresponded to capillary condensation within uniform mesopores. At relative pressures above 0.9, a slight hysteresis loop was observed for the calcined

TABLE 1: Textural Characteristics of the Calcined MCM-41 Samples

hydrothermal temperature/time[a]	BET surface area (m^2/g)	average pore diameter D_{BJH} (nm)	pore volume (mL/g)	pore spacing d_{100}(nm)	cell parameter a_0(nm)	pore wall thickness t^b (nm)
100 °C/24h	1030	3.71	0.956	4.164	4.81	1.10
100 °C/48h	957	4.26	1.020	4.232	4.89	0.63
160 °C/24h	851	5.41	1.150	nd	nd	nd

[a] Only hydrothermal conditions are changed according to the experimental section while the other processes are the same. [b] Pore wall thickness $t = a_0 - D_{BJH}$; nd: not determined.

TABLE 2: Main Chemical Compositions of the Samples (wt %)

samples	SiO_2	MgO	Fe_2O_3	Al_2O_3	CaO	K_2O	Na_2O
original attapulgite	53.64	11.87	2.68	7.45	2.21	0.46	0.082
acid-leached attapulgite	74.31	0.57	0.34	5.02	0.12	0.30	0.043

MCM-41, which was possibly associated with condensation in textural porosity.[48] The position of the capillary condensation with respect to the P/P_0 axis was directly related to the diameter of the mesopore, and the steepness of this step indicated the well-ordered mesopore structure and the uniformity of the pore size distribution.[15] The average pore size was around 3.7 nm with range of 2−5 nm in diameter (Figure 6), with the pore size distribution of the calcined sample centered at about 2.6 nm. As expected for the as-synthesized silica−surfactant mesophase, the surface area and pore volume were only 60% of the corresponding values measured for the calcined Al-MCM-41. The isotherms showed an obvious H4 loop typical of slit-type pore channels in the isotherm (Figure 5). In addition, the slope of the capillary condensation step at $P/P_0 = 0.25-0.35$ for the as-synthesized sample was clearly less than that at the same P/P_0 range for the calcined material, indicating a lower degree of structural order for the as-synthesized sample.[16]

Significantly, grinding and acid-leaching did not modify the shape of the isotherms compared with the untreated attapulgite; only an increase in initial uptake was apparent, similar to previous observations.[47] The ground and acid-leached samples did not show any capillary condensation step in the N_2 adsorption−desorption isotherms or well-defined pore size distribution curves, although a slight H3 and H4 type hysteresis were observed at a pressure above 0.8. However, the surface area of the untreated attapulgite sample decreased from 182 m^2/g

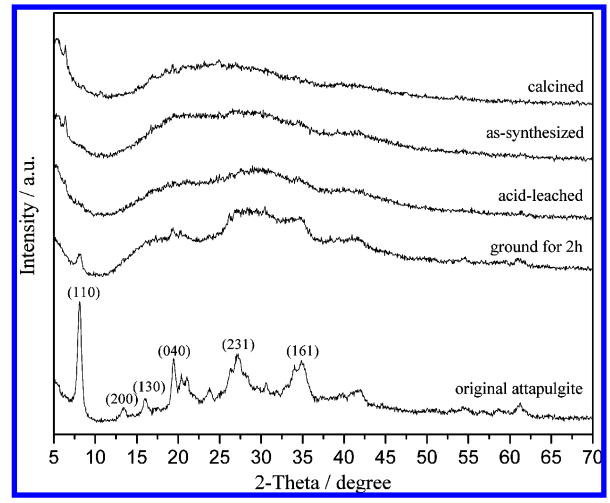

Figure 4. WAXRD patterns of the samples.

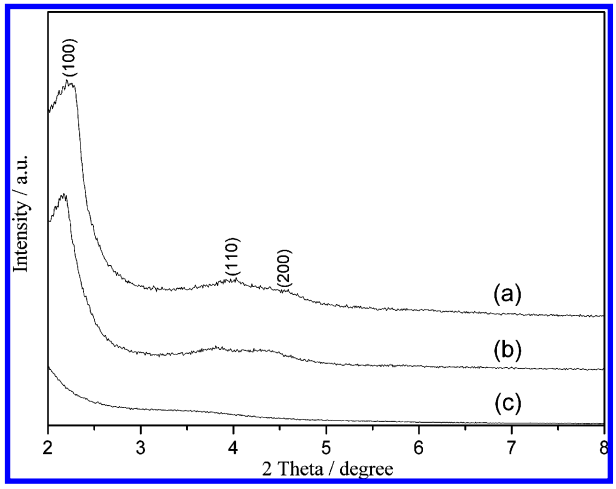

Figure 2. SAXRD patterns of the calcined Al-MCM-41 via hydrothermally heating the acid-leached samples at different temperatures/times: (a) 100 °C/24 h; (b) 100 °C/48 h; (c) 160 °C/24 h.

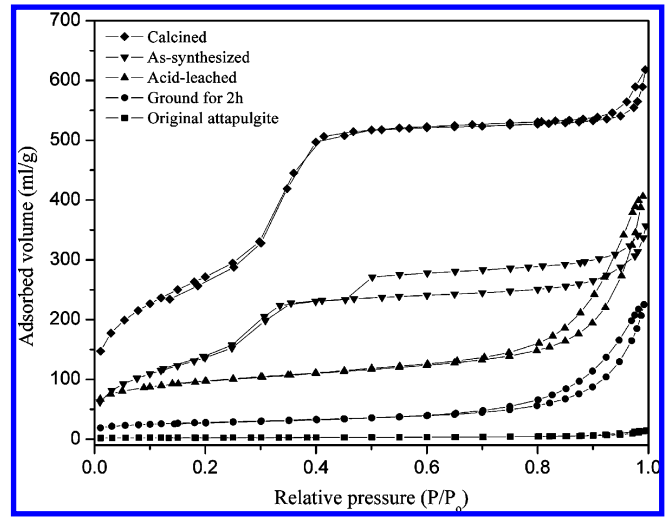

Figure 5. N_2 adsorption−desorption isotherms and pore size distribution of the samples.

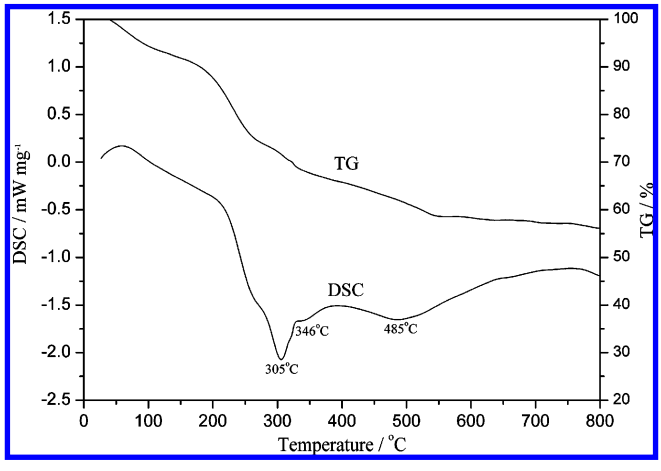

Figure 3. TG-DSC curves of the as-synthesized sample.

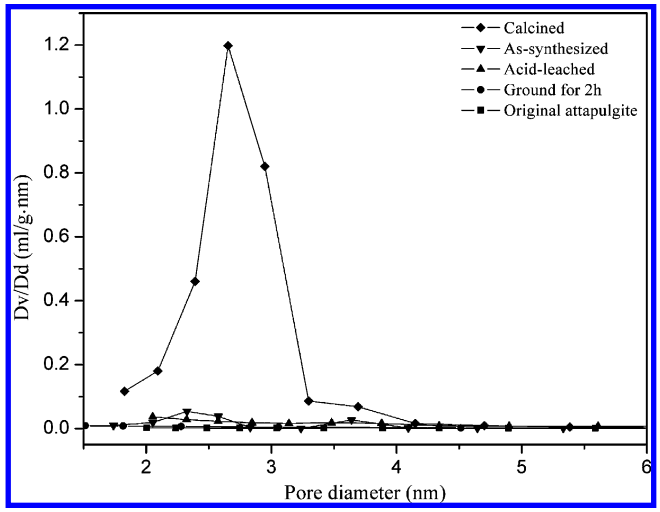

Figure 6. Pore size distribution of the samples.

TABLE 3: Summary of Surface Area, Pore Diameter, and Pore Volume of the Samples

samples	BET surface area (m^2/g)	average pore diameter (nm)	pore volume (mL/g)
original attapulgite	182	10.84	0.492
ground for 2 h	111	12.05	0.333
acid-leached	317	7.94	0.629
as-synthesized	603	3.66	0.552
calcined	1030	3.71	0.956

to a value of 111 m^2/g after grinding (Table 3), consistent with transformation of the layered microporous structure to a more compact amorphous phase (Figure 4). Similar observations have been reported for ground samples of Illite,[49] sepiolite,[42] and imogolite.[50] Significantly, after acid treatment, the sample had a surface area of 317 m^2/g, which was nearly 3 times that of the ground sample. The large increase in surface area was attributed primarily to acid-induced leaching of Mg^{2+}, Fe^{3+}, and Al^{3+} ions from the octahedral sites to increase levels of microporosity. Indeed, the average pore diameter decreased from 12 nm for ground attapulgite to about 8 nm for the acid-leached sample, but the pore volume increased to nearly twice that of original attapulgite (Table 3).

The surface areas of the Al-MCM-41 products were dependent on various factors including grinding time, hydrothermal parameters (temperature and time), and calcination temperature. Successful preparation of Al-MCM-41 from attapulgite was achieved using increased grinding times, but the BET surface areas of the calcined samples were significantly reduced. For example, surface areas of 914 m^2/g and 888 m^2/g were determined for products prepared using grinding times of 4 or 6 h, respectively, compared with 1030 m^2/g for the calcined Al-MCM-41 synthesized from attapulgite ground for 2 h. To some extent, the decreased surface areas of the products were related to the lower BET surface area of the ground samples (72 m^2/g for 4 h grinding and 55 m^2/g for 6 h grinding) compared with that of 2 h-ground attapulgite (111 m^2/g) (Table 3). On the other hand, the crystallinity of the 4 h-ground sample and 6 h-ground sample calculated from XRD patterns (data not shown) was only 15% and 8%, respectively, lower than that of 2 h-ground attapulgite (31.5%), indicating that prolonged grinding resulted in a high degree of degradation of the original attapulgite.

The effect of calcination temperature on the porosity of the calcined Al-MCM-41 materials was systematically investigated. Samples calcined at 450, 540, 600, 700, and 800 °C had BET surface areas of 917, 1030, 887, 890, and 921 m^2/g, respectively. The pore volume decreased with increasing calcination temperature, and was reduced to 0.776 mL/g for the Al-MCM-41 sample treated at 800 °C. In this case, the average pore diameter was only 3.37 nm, indicating a partial collapse of the mesopores.

Morphological Evolution. TEM and FESEM studies were undertaken to reveal changes in the shape and size of particles associated with the transformation of natural attapulgite to Al-MCM-41 upon grinding, acid treatment, hydrothermal synthesis and subsequent calcination (Figure 7). Typically, TEM images of the attapulgite starting material showed bunches of fibers with widths of around 150 nm and lengths of a few micrometers (Figure 7a). Single fibers were approximately 30 nm in diameter and 1.3 μm in length (Figure 7b). After grinding, the fiber bundles were disaggregated, and single filaments were "cold-welded" into agglomerates of short-rod like particles with widths and lengths in the range of 35−60 nm and 100−150 nm,[43] respectively (Figure 7c). The results were consistent with the decrease in surface area from 182 m^2/g for natural attapulgite to 111 m^2/g for the ground sample (Table 3), as well as the amorphization of the sample as determined by WAXRD (Figure 4). Similar morphological changes have been reported during grinding of imogolite.[50]

Acid leaching of the ground attapulgite had a marginal effect on particle shape and size, although the process resulted in moderate disaggregation of the short rod-like particles (Figure 7d), along with an increase in the surface area (Table 3) due mainly to the removal of magnesium cations. On the other hand, there were moderate changes in texture and adsorption properties (Figure 4 and 5). In contrast, when natural attapulgite was subjected to direct acid attack without preliminary grinding, the treated samples retained their fibrous morphology.[47] Similarly, studies on saponite reported no change in morphology under acid treatment even though the lamellar (smectitic) structure was almost completely lost.[51] The results confirmed that grinding pretreatments play a key role in the materials processing of natural clay minerals.

TEM images of the as-synthesized samples showed an irregular morphology with reticular structure (Figure 7e), which was associated with formation of a silica−surfactant mesophase[19] with a surface area (603 m^2/g) almost twice that of the ground sample (Table 3). After calcination, the TEM micrographs showed evidence of banana-shaped particles consisting of a hexagonally ordered array of mesostructured channels about 4 nm in width (Figure 7f−h and Figure 1).

FTIR Spectra. Further information on the transformation of natural attapulgite to Al-MCM-41 was obtained by FTIR spectroscopy (Figure 8). Grinding the natural mineral for 2 h resulted in a broadening of the stretching vibrations at 1027 cm^{-1} ((Mg,Al)−O−Si) and 987 cm^{-1} (Si−O−Si(Al)), indicating that structural destruction first occurred at the interface between the octahedral and tetrahedral sheets due to the relative weakness of the (Mg,Al)-O linkages in this region of the structure.[52] In contrast, (Mg,Al)−O vibrations at 3610 cm^{-1} remained unchanged after 2 h of grinding, suggesting increased resistance of the inner (Mg,Al)-O units of the octahedral sheets. Likewise, the Si−O in-plane vibrations at 480 cm^{-1} and 1026 cm^{-1} did not change noticeably after grinding the samples, suggesting that the basal planes of the tetrahedral units remained relatively intact. Similar observations were also reported for the grinding of Illite.[5] Significantly, FTIR spectra showed a shift in the shoulder peak at 1194 cm^{-1} (Si−O stretch) for natural attapulgite to a value of 1188 cm^{-1} for the ground sample

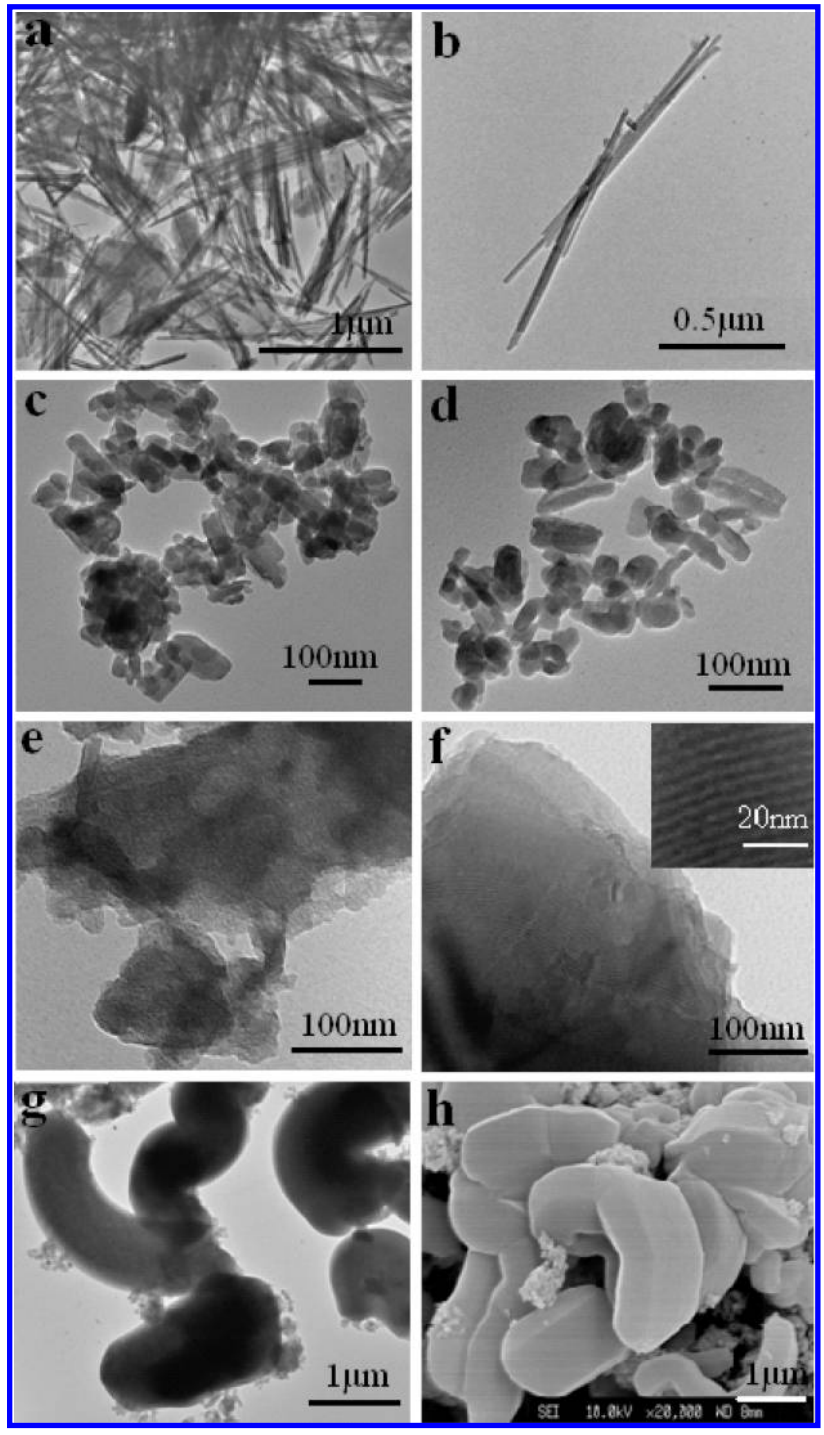

Figure 7. TEM images of the samples: (a) fiber-bundles and (b) single fiber of original attapulgite; (c) ground for 2 h; (d) acid-leached; (e) as-synthesized; (f) calcined Al-MCM-41 (inset is amplified hexagonal array of the mesostructured channels); and (g) calcined Al-MCM-41 at low magnification. (h) FESEM image of calcined Al-MCM-41.

(Figure 8). The decrease in wavenumber was attributed to the substitution of Al^{3+} ions for Si^{4+} in $[SiO_4]^{4-}$ tetrahedral to form $[AlO_4]^{5-}$ tetrahedra with increased electronegativity (see also NMR results, below). As the Al−O bond length (0.175 nm) is greater than that of Si−O (0.162 nm), the force constant (k) and vibration frequency (ν) is decreased ($\nu^2 = k(\pi c)^2/(4\mu)$; μ = atomic weight, c = speed of light[53]) by Al^{3+} substitution into the tetrahedral layer.

Acid leaching and amorphization resulted in a shift of the 1650 cm^{-1} bending mode to 1630 cm^{-1} (Figure 8), confirming transformation of bound water to weakly bound hydroxyl groups. A very broadband at 3500−3200 cm^{-1} was observed in the acid-leached sample that possibly involved stretching vibrations of a randomly attached hydroxyl group on the new amorphous phase created by acid attack. A band at 952 cm^{-1} was assigned to the stretching vibration of amorphous silica, formed through polycondensation of $[SiO_4]$ tetrahedral under acid conditions.[50] The in-plane Si−O stretching mode at 1026 cm^{-1} for natural attapulgite and the ground sample was shifted to an out-of-plane Si−O stretching vibration at 1093 cm^{-1} in the acid-leached sample, consistent with the transformation of Si−OMg(Al) linkages into Si−OH.[54] Additionally, a new band at 797 cm^{-1} due to Si−OH vibration was formed. These results were in agreement with the XRD analysis and indicated that

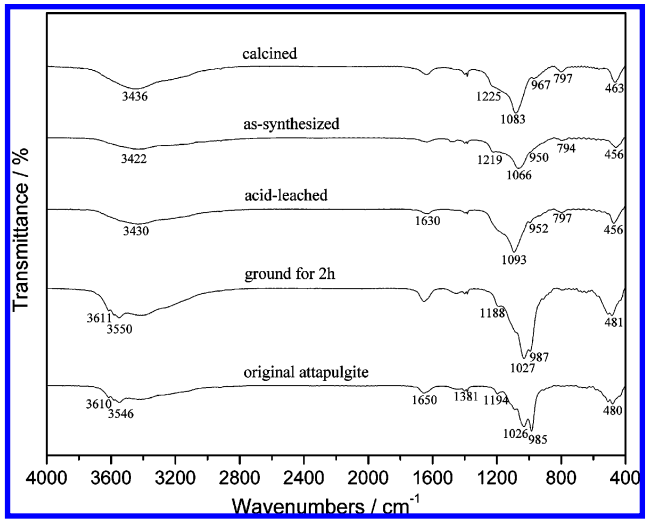

Figure 8. FTIR spectra of the samples.

the increase in number of Si−OH groups was responsible for changes in the surface properties of the acid-treated attapulgite and facilitated the extraction of cations, which resulted in structural collapse.

FTIR spectra of the calcined MCM-41 products were very similar to the results reported previously.[15] The internal and external asymmetric Si−O stretching vibrations at 1066 cm^{-1} and 1219 cm^{-1} for the as-synthesized sample were shifted to higher wavenumbers at 1083 cm^{-1} and 1225 cm^{-1}, respectively, for the calcined MCM-41. Similarly, the band at 456 cm^{-1} assigned to a tetrahedral Si−O bending vibration also shifted to higher wavenumbers after calcination. These shifts were consistent with the formation of new Si−O−Si and Si−O−Al bonds during thermal treatment. Simultaneously, a new band was observed in the calcined material at 967 cm^{-1} (Si−O− group stretch) reflecting the increased structural stabilization of MCM-41 upon thermal treatment.[55]

^{29}Si and ^{27}Al MAS NMR Spectra. The ^{29}Si MAS NMR spectrum (Figure 9a) for natural attapulgite showed resonance signals in the range of −91 to −98 ppm corresponding to fully condensed $Q^4(0Al)$ SiO_4, $Q^4(1Al)$ ($(SiO_3)Si(OAl)$), or possible $(SiO)_3Si(OMg)$ in the tetrahedral sheet.[56] After grinding, a new low-intensity peak at −102 ppm attributed to Q^3 ($(SiO)_3Si(OH)$) was observed along with the wide Q^4 resonance at 110 ppm, indicating that the Si−O bonded layered structure was partially maintained after mechanical grinding even though the morphology was significantly modified. The ^{29}Si MAS NMR spectrum for the acid-leached sample showed three signals at −111 ppm, −102 ppm, and −97 ppm, corresponding to Q^4, Q^3, and Q^2 ($(SiO)_2Si(OH)_2$) environments, respectively (Figure 9a). The emergence of the sharp and intense peak at −111 ppm indicated formation of bonded four-coordinated silicon (amorphous SiO_2) from the residual Si−O framework after the removal of Mg^{2+}, Al^{3+}, and Fe^{3+} under acid attack,[57] in accordance with the FTIR results. The presence of a signal with increased intensity at −102 ppm was due to the partial transformation from $(SiO)_3Si(OMg)$ to $(SiO)_3Si(OH)(Q^3)$, again, in agreement with FTIR spectra (Figure 8).

^{29}Si MAS NMR spectra of the as-synthesized and calcined MCM-41 samples showed broad resonances that were consistent with the presence of amorphous silica, suggesting an irregular local arrangement of Si−O−Si bonds at the pore walls and a broad range of Si−O−Si bond angles within the materials (Figure 9a).[58] This result was in agreement with the WAXRD and FTIR results. Gaussian fitted spectra showed three signals

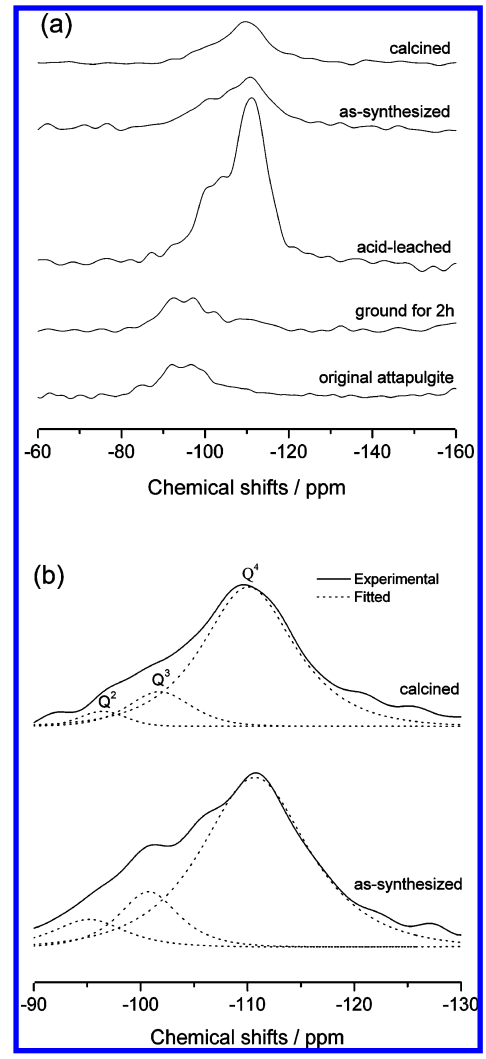

Figure 9. (a) ^{29}Si NMR spectra of the samples from original attapulgite to calcined Al-MCM-41. (b) Experimental and fitted Gaussian curves for ^{29}Si NMR spectra of the as-synthesized and calcined samples.

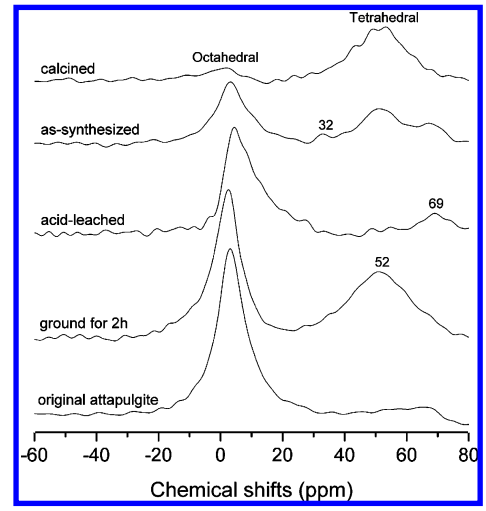

Figure 10. ^{27}Al MAS NMR spectra of the samples.

at −111 ppm, −102 ppm and −97 assigned to Q^4, Q^3 and Q^2, respectively (Figure 9b). The ^{29}Si NMR spectrum of the calcined MCM-41 was identical to data in previous reports.[1,12,14,15] A weak signal at −106 ppm possibly corresponded to a pentahedrally coordinated aluminum of Si(3Si,Al) in four samples, but absent in the calcined MCM-41 sample (Figure 9a). The

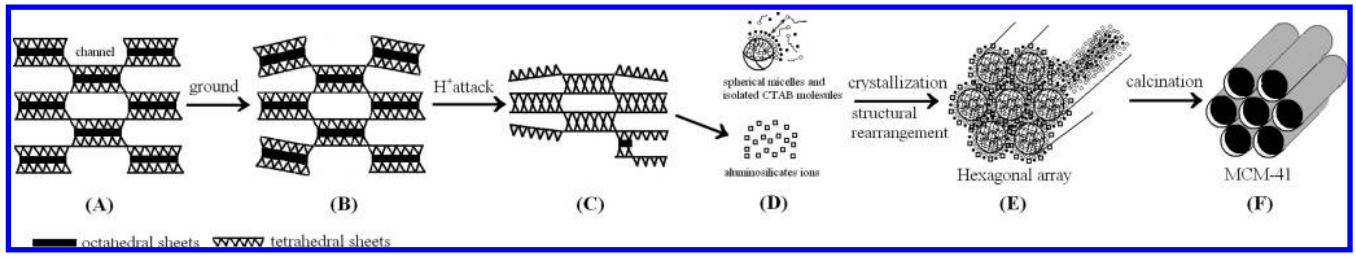

Figure 11. Proposed mechanism from natural attapulgite to mesoporous material Al-MCM-41: (A) original attapulgite; (B) ground attapulgite; (C) acid-leached sample; (D) reactants for hydrothermal synthesis; (E) as-synthesized sample; (F) calcined sample Al-MCM-41.

presence of Al atoms in the MCM-41 network generates Si(3Si,Al) and Si(2Si,2Al) environments, which would also contribute to the resonance peak intensities at −102 ppm and −97 ppm.[58] Quantitative analysis was not undertaken because the peaks were broad and overlapping.

^{27}Al MAS NMR spectra of the samples at various stages in the transformation process are shown in Figure 10. In general, the intensity and width of the sharp resonance peak at 3 ppm in natural attapulgite, corresponding to octahedral coordinated nonframework Al^{3+} ions, decreased progressively from natural attaulgite to the MCM-41 product due to structural degradation arising from mechanical shearing, acid-induced leaching of Mg^{2+} and Fe^{3+} from the Mg(Al,Fe)-O octahedral sites, hydrothermal synthesis, and calcination. Grinding resulted in an intense, broad resonance at 52 ppm, which was attributed to tetrahedrally coordinated aluminum,[56] suggesting partial replacement of Si by Al in the tetrahedral layer, in accordance with the FTIR spectroscopy results. Acid leaching resulted in upfield shifts in the octahedral and tetrahedral Al resonances from 3 ppm to 7 ppm, and 52 ppm to 69 ppm, respectively, suggesting further structural rearrangements in the Si−O and Mg(Al,Fe)-O networks.

The ^{27}Al MAS NMR spectrum of the as-synthesized sample showed two main resonances at 52 ppm (four-coordinate framework Al^{3+}) and close to 3 ppm (six-coordinate extra-network/nonframework Al^{3+} ions, possibly as $[Al(H_2O)_6]^{3+}$ inside the pores). A weak signal at 32 ppm was assigned provisionally to a pentahedrally coordinated network aluminum species.[58−60] After calcination, the spectrum showed an intense resonance for tetrahedrally coordinated Al^{3+}, absence of the penta-coordinated Al^{3+} sites, and a very weak signal for Al^{3+} in octahedral sites (Figure 10). The results confirmed that calcination enhanced the stability of Al^{3+} ions within the tetrahedral framework and facilitated migration of both the penta- and hexa-coordinated Al^{3+} ions into the tetrahedral sites in the amorphous Al-MCM-41 framework, which was responsible for the absence of signal around −106 ppm due to Si(3Si,Al) for the calcined MCM-41 sample, but present in the other four samples (Figure 9). The results were in good agreement with previous reports.[12,14,15,58,59] In addition, a small peak at around 42 ppm was visible in the spectrum of the calcined material that we tentatively attribute to four-coordinate extra-network aluminum, in agreement with the formation of Si−O−Al linkages observed in the corresponding FTIR spectrum (Figure 8), and on the basis of previous reports on dealuminated zeolites.[59] The above results indicate that the tetrahedral network of attapulgite is retained when subjected to sequential grinding, acid-leaching, hydrothermal reaction, and calcination, and provides the necessary framework and source of building blocks for construction of the final Al-MCM-41 product.

Proposed Mechanism from Natural Attapulgite to Mesoporous Materials MCM-41. On the basis of the above analysis, we suggest the following mechanism for the preparation of mesoporous materials from natural attapulgite (Figure 11). First, grinding leads to amorphization of the layered structure of natural attapulgite (Figure 11A), in which fibrous bundles of attapulgite are transformed into rod-like particles and both surface area and pore volume are reduced due to partial breakdown and disordering of the mineral structure (Figure 11B). Significantly, this process results in migration of a fraction of the Al^{3+} ions into the Si−O tetrahedral sheets. Subsequent acid leaching produces progressive dissolution of the octahedral sheet and removal of their constituent Mg^{2+}, Fe^{3+}, and Al^{3+} ions without change in the morphology of the rod-shaped particles, formation of amorphous silica on the surface of the layered silicate remnants due to polycondensation of the Si−O tetrahedral sheets, and surface adsorption of octahedrally coordinated Al^{3+} species such as $[Al(H_2O)_6]^{3+}$ (Figure 11C). As a consequence, the acid-treated material exhibits microporosity, an increase in surface area and pore volume, a decrease in average pore diameter (from 12 to 7.9 nm), and an increase in the numbers of surface silanol groups along with $[Al(H_2O)_6]^{3+}$ species (Figure 11D). Hydrothermal reaction of this material with an alkaline solution of aqueous CTAB produces a hexagonally ordered silica−surfactant mesophase solution (Figure 11E) by a conventional templating mechanism,[61−63] in which the acid-treated sample acts as a source of both Al and Si building blocks that undergo condensation within the interstitial regions of the surfactant lyotropic mesophase. Interestingly, while the as-synthesized material consists of significant amounts of octahedrally coordinated Al^{3+} sites, these are effectively absent after removal of the surfactant template by calcination (Figure 11F).

Conclusions

Ordered aluminum-containing mesoporous materials Al-MCM-41 with surface areas of around 1030 m^2/g and average pore diameter of 3.7 nm have been successfully synthesized via hydrothermal treatment of ground, acid-leached attapulgite. Preliminary grinding and acid leaching were shown to be critical for ensuring the necessary textural/structural characteristics of the Al-MCM-41 products. Grinding resulted in structural amorphization and morphological transformation of natural attapulgite, and induced Al^{3+} ions to enter the tetrahedral sheet acting as a framework ion via replacing of Si atoms in $[SiO_4]$ units. The textual variations of ground attapulgite subjected to acid attack were associated with modifications in the undestroyed silicate fragments and the silica particles created during substantial dissolution of the octahedral sheets. As a consequence, the silicate sheets in attapulgite can retain the skeletal structure of the mineral after grinding and acid-leaching, and thus provide the necessary building blocks for the surfactant-templated hydrothermal synthesis of Al-MCM-41. The calcined Al-MCM-41 product consists of amorphous silica with Al^{3+} ions mainly in tetrahedral sites. Our results indicate that the synthesis of MCM-41 materials from pretreated attapulgite gives products

on par with those synthesized by conventional routes using tetraalkoxysilanes. Thus, our method could offer a more benign approach to the general production of MCM-41 materials for diverse functional applications.

Acknowledgment. This work was supported by the UK foundation and NSFC (50774095).

Supporting Information Available: WAXRD patterns, textural characteristics, and N_2 adsorption−desorption isotherms of the samples from original attapulgite to porous materials without grinding. This material is available free of charge via the Internet at http://pubs.acs.org.

References and Notes

(1) Beck, J. S.; Vartuli, J. C.; Roth, W. J.; Leonowicz, M. E.; Kresge, C. T.; Schmitt, K. D.; Chu, C. T.-W.; Oison, D. H.; Sheppard, E. W.; McCullen, S. B.; Higgins, J. B.; Schlenker, J. L. *J. Am. Chem. Soc.* **1992**, *114*, 10834–10843.

(2) Kresge, C. T.; Leonowicz, M. E.; Roth, W. J.; Vartuli, J. C.; Beck, J. S. *Nature* **1992**, *359*, 710–712.

(3) Hu, Y.; Martra, G.; Zhang, J.; Higashimoto, S.; Coluccia, S.; Anpo, M. *J. Phys. Chem. B* **2006**, *110*, 1680–1685.

(4) Perathoner, S.; Lanzafame, P.; Passalacqua, R.; Centi, G.; Schlgöl, R.; Su, D. S. *Microporous Mesoporous Mater.* **2006**, *90*, 347–361.

(5) He, J.; Ma, K.; Jin, J.; Dong, Z.; Wang, J.; Li, R. *Microporous Mesoporous Mater.* **2009**, *121*, 173–177.

(6) Shimizu, Y.; Hyodo, T.; Egashira, M. *J. Eur. Ceram. Soc.* **2004**, *24*, 1389–1398.

(7) Parala, H.; Winkler, H.; Kolbe, M.; Wohlfart, A.; Fischer, R. A.; Schmechel, R.; von Seggern, H. *Adv. Mater.* **2000**, *12*, 1050–1055.

(8) Lee, K. P.; Showkat, A. M.; Gopalan, A. I.; Kim, S. H.; Choi, S. H. *Macromolecules* **2005**, *38*, 364–371.

(9) Sun, Y.; Liu, X. W.; Su, W.; Zhou, Y.; Zhou, L. *Appl. Surf. Sci.* **2007**, *253*, 5650–5655.

(10) Angelos, S.; Liong, M.; Choi, E.; Zink, J. I. *Chem. Eng. J.* **2008**, *137*, 4–13.

(11) Okada, K.; Yoshizaki, H.; Kameshima, Y.; Nakajima, A.; Madhusoodana, C. D. *J. Colloid Interface Sci.* **2007**, *314*, 176–183.

(12) Melo, R. A. A.; Giotto, M. V.; Rocha, J.; Urquieta-González, E. A. *Mater. Res.* **1999**, *2*, 173–179.

(13) Gaydhankar, T. R.; Samuel, V.; Joshi, P. N. *Mater. Lett.* **2006**, *60*, 957–961.

(14) Luan, Z.; Cheng, C.-F.; Zhou, W.; Klinowski, J. *J. Phys. Chem.* **1995**, *99*, 1018–1024.

(15) Wang, G.; Wang, Y.; Liu, Y.; Liu, Z.; Guo, Y.; Liu, G.; Yang, Z.; Xu, M.; Wang, L. *Appl. Clay Sci.* **2009**, *44*, 185–188.

(16) Amama, P. B.; Lim, S.; Ciuparu, D.; Pfefferle, L.; Haller, G. L. *Microporous Mesoporous Mater.* **2005**, *81*, 191–200.

(17) Linssen, T.; Cassiers, K.; Cool, P.; Lebedev, O.; Whittaker, A.; Vansant, E. F. *Chem. Mater.* **2003**, *15*, 4863–4873.

(18) Kimura, T.; Kuroda, K. *Adv. Funct. Mater.* **2009**, *19*, 511–527.

(19) Yang, H.; Du, C.; Jin, S.; Tang, A.; Li, G. *Microporous Mesoporous Mater.* **2007**, *102*, 204–211.

(20) Yanagisawa, T.; Shimizu, T.; Kuroda, K.; Kato, C. *Bull. Chem. Soc. Jpn.* **1990**, *63*, 988–992.

(21) Fukushima, Y.; Inagaki, S. *Mater. Sci. Eng., A* **1996**, *217*−*218*, 116–118.

(22) Inagaki, S.; Fukushima, Y.; Kuroda, K. *Chem. Commun.* **1993**, 680–682.

(23) Kang, F.; Wang, Q.; Xiang, S. *Mater. Lett.* **2005**, *59*, 1426–1429.

(24) Liu, J.; Jiang, Y.; Wang, A.; Song, B. *J. Inorg. Mater.* **2003**, *18*, 867–871.

(25) Tang, Y.; Jiang, T.; Zhang, R.; Zhao, Q.; Yin, H. *Nanotechnol. Precis. Eng.* **2008**, *6*, 185–189.

(26) Bradley, W. F. *Am. Mineral.* **1940**, *25*, 405–413.

(27) Haden, W. L.; Schwint, I. A. *Ind. Eng. Chem.* **1967**, *59*, 58–69.

(28) Murray, H. H. *Appl. Clay Sci.* **2000**, *17*, 207–221.

(29) Cao, J.-L.; Shao, G.-S.; Wang, Y.; Liu, Y.; Yuan, Z.-Y. *Catal. Commun.* **2008**, *9*, 2555–2559.

(30) Liu, Y.; Liu, P.; Su, Z.; Li, F.; Wen, F. *Appl. Surf. Sci.* **2008**, *255*, 2020–2025.

(31) Liu, Y.; Liu, P.; Su, Z. *Polym. Int.* **2008**, *57*, 306–310.

(32) Pan, B.; Ren, J.; Yue, Q.; Liu, B.; Zhang, J.; Yang, S. *Polym. Compos.* **2009**, *30*, 147–153.

(33) Wang, W.; Zheng, Y.; Wang, A. *Polym. Adv. Technol.* **2008**, *19*, 1852–1859.

(34) Shi, L.; Yao, J.; Jiang, J.; Zhang, L.; Xu, N. *Microporous Mesoporous Mater.* **2009**, *122*, 294–300.

(35) Kang, Y.; Zhu, H.; Yang, G.; Guo, X.; Hou, W.; Yan, Q.; Gu, M.; Hu, C. *Adv. Funct. Mater.* **2004**, *14*, 816–820.

(36) Tanev, P. T.; Pinnavaia, T. J. *Science* **1995**, *267*, 865–867.

(37) de Juan, F.; Ruiz-Hitzky, E. *Adv. Mater.* **2000**, *12*, 430–432.

(38) Suquet, H. *Clay Clay Miner.* **1989**, *37*, 439–445.

(39) Yang, H.; Du, C.; Hu, Y.; Jin, S.; Yang, W.; Tang, A.; Avvakumov, E. G. *Appl. Clay Sci.* **2006**, *31*, 290–297.

(40) Aglietti, E. F.; Porto López, J. M. *Mater. Res. Bull.* **1992**, *27*, 1205–1216.

(41) Pérez-Rodríguez, J. L.; Madrid Sánchez Del Villar, L.; Sánchez-Soto, P. J. *Clay Miner.* **1988**, *23*, 399–410.

(42) Cornejo, J.; Hermosin, M. C. *Clay Miner.* **1988**, *23*, 391–398.

(43) Sánchez-Soto, P. J.; Wiewióra, A.; Avilés, M. A.; Justo, A.; Pérez-Maqueda, L. A.; Pérez-Rodríguez, J. L.; Bylina, P. *Appl. Clay Sci.* **1997**, *12*, 297–312.

(44) Lin, I. J.; Nadiv, S. *Mater. Sci. Eng.* **1979**, *39*, 193–209.

(45) Corma, A.; Mifsud, A.; Sanz, E. *Clay Miner.* **1990**, *25*, 197–205.

(46) Deng, J.; Fan, K. In *Physical Chemistry*; Higher Education Press: Beijing, 1993; pp 465−467.

(47) Gonzalez, F.; Pesquera, C.; Benito, I.; Mendioroz, S.; Pajares, J. A. *Clay Clay Miner.* **1989**, *37*, 258–262.

(48) Gianotti, E.; Bertolino, C. A.; Benzi, C.; Nicotra, G.; Caputo, G.; Castino, R.; Isidoro, C.; Coluccia, S. *Appl. Mater. Interfaces* **2009**, *1*, 678–687.

(49) Yang, H.; Yang, W.; Hu, Y.; Du, C.; Tang, A. *Part. Part. Syst. Charact.* **2005**, *22*, 207–211.

(50) Henmi, T.; Yoshinaga, N. *Clay Miner.* **1981**, *16*, 139–149.

(51) Bisio, C.; Gatti, G.; Boccaleri, E.; Marchese, L.; Bertinetti, L. *Langmuir* **2008**, *24*, 2808–2819.

(52) Yao, C.; Zeng, Y.; Chen, Z.; Li, W.; Li, X.; Xu, Q. *J. Chin. Ceram. Soc.* **2009**, *37*, 485–491.

(53) Lu, W. In *Infrared Spectrum of Minerals*; Chongqing University Press: Chongqing, China, 1989; pp 70−115.

(54) Lubguban, J.; Kurate, Y., Jr.; Inokuma, T.; Hasegawa, S. *J. Appl. Phys.* **2000**, *87*, 3715–3722.

(55) Camblor, M. A.; Corma, A.; Pérez-Pariente, J. *J. Chem. Soc., Chem. Commun.* **1993**, *6*, 557–559.

(56) He, H.; Guo, J.; Xie, X.; Lin, H.; Li, L. *Clay Miner.* **2002**, *37*, 337–344.

(57) Temuujin, J.; Okada, K.; MacKenzie, K. J. D.; Jadambaa, Ts. *Powder Technol.* **2001**, *121*, 259–262.

(58) Liepold, A.; Roos, K.; Reschetilowski, W.; Esculcas, A. P.; Rocha, J.; Philippou, A.; Anderson, M. W. *J. Chem. Soc., Faraday Trans.* **1996**, *92*, 4623–4629.

(59) Rocha, J.; Klinowski, J. *Chem. Phys. Lett.* **1991**, *187*, 401–408.

(60) De Witte, B. M.; Grobet, P. J.; Uytterhoeven, J. B. *J. Phys. Chem.* **1995**, *99*, 6961–6965.

(61) Monnier, A.; Schüth, F.; Huo, Q.; Kumar, D.; Margolese, D.; Maxwell, R. S.; Stucky, G. D.; Krishnamurty, M.; Petroff, P.; Firouzi, A.; Janicke, M.; Chmelka, B. F. *Science* **1993**, *261*, 1299–1303.

(62) Huo, Q.; Margolese, D. I.; Ciesla, U.; Feng, P.; Gier, T. E.; Sieger, P.; Leon, R.; Petroff, P. M.; Schüth, F.; Stucky, G. D. *Nature* **1994**, *368*, 317–321.

(63) Ruiz-Hitzky, R.; Letaïef, S.; Prévot, V. *Adv. Mater.* **2002**, *14*, 439–443.

JP911516B